The Magnetic Field Distributions from a Propagating Action Potential: Results from a Preliminary Model Study

Prepared by:
Mark Trew & Andrew Pullan

Auckland Bioengineering Institute
The University of Auckland
New Zealand

23 January 2007

1.0 Introduction

This study computed magnetic flux density fields corresponding to a spreading action potential in a simulated slab of cardiac tissue. The tissue was located in a bath and the stimulus was generated through an extracellular cathode within the tissue and an anode located in the bath solution below the tissue sample. The problem was based on dimensions and parameters provided by Dr. Franz Baudenbacher, 30 November 2006.

2.0 Methods

2.1 Computational Mesh

The problem was comprised of a cardiac tissue slab of dimensions 30 mm by 30 mm by 1 mm placed in a conducting saline bath (Figure 1A-1C). The total domain of dimension 80 mm by 80 mm by 2.05 mm (Figure 1) was discretized into 3x3x4 = 36 finite elements (Figure 2). These elements described the bath, tissue, tissue and bath layers through the depth of the model (Figure 2B) and the bath, tissue and bath regions in the plan view (Figure 2A).

Each element was sub-discretized (to the resolution indicated in Figure 2) to provide the computational mesh used for solving for transmembrane potentials and extracellular potentials, and the magnetic flux density fields. The sub-element discretization was graded to provide computational resolution where most needed and in order to reduce the overall number of degrees of freedom (Figure 2). The mesh was coarsest in the bath region and finest near the interfaces between bath and tissue and in the tissue above the stimulating electrode (Figure 1D). The total number of computational points was 13725638. Two potentials were solved at each point.

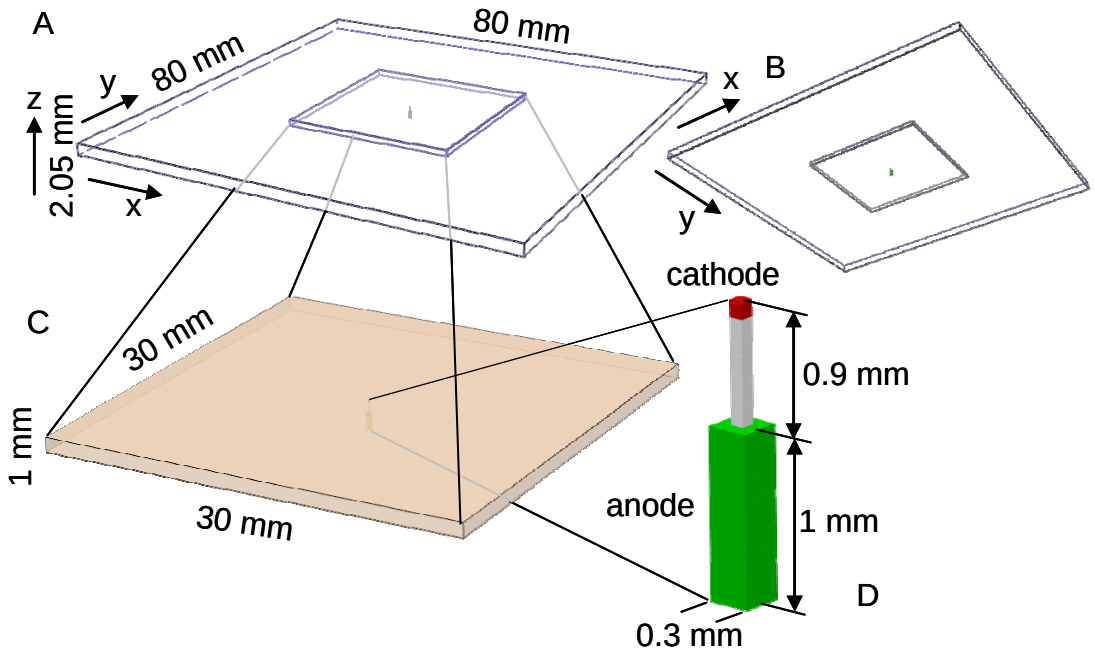

Figure 1. Problem dimensions. A. View of tissue slab in bath. Bath is 0.05 mm thick above tissue. B. View from below. Bath is 1 mm thick below tissue. C. Dimensions of tissue slab. D. Exploded view of electrode. The cathode is located 0.1 mm below the tissue surface. The anode is located in the bath below the tissue slab.

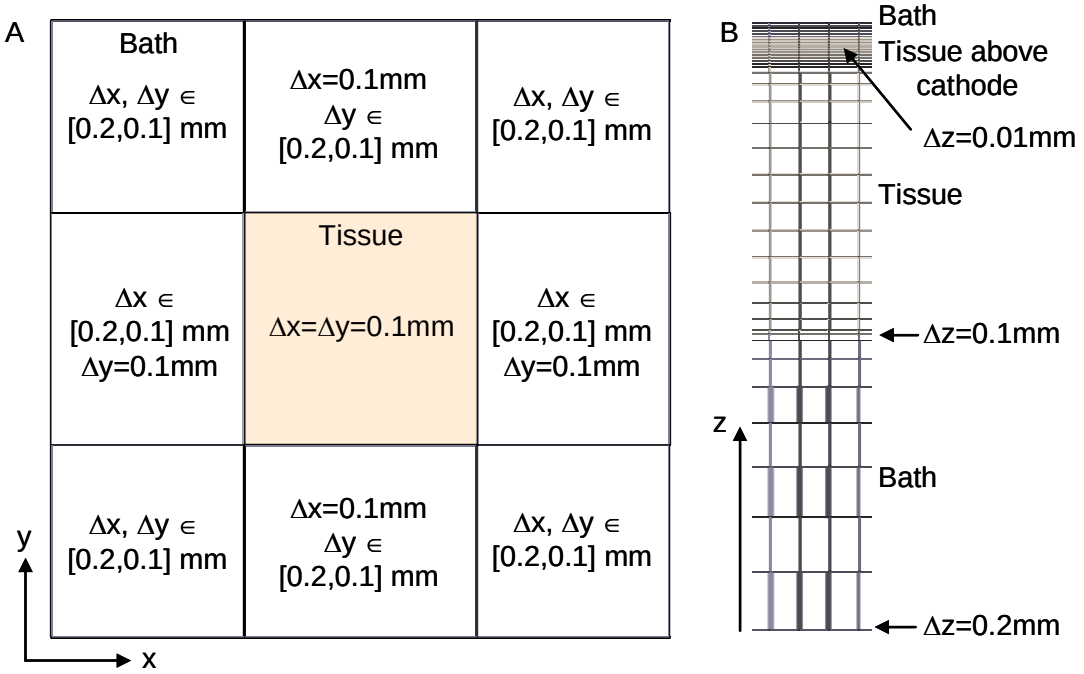

Figure 2. Examples of the graded computational mesh. A. Plan view. B. Elevation. A fine mesh in z was used in the 0.05 mm bath layer above the tissue and in the 0.1 mm tissue layer above the cathode.

2.2 Computing Electric Potentials

The transmembrane, V_m, and extracellular, ϕ, potential fields were computed by solving the bidomain equations. The current densities in the intracellular and extracellular spaces were computed from the gradients of the potential fields and the effective conductivity tensor fields [7]. The biodomain equations were discretised in space using a finite volume method devised to solve large problems [5]. A first-order operator splitting algorithm (e.g. [1]) was used to progress in time, with a Crank-Nicholson implicit time discretization of the parabolic problem. A time step of 0.05 ms was utilized. The resulting linear systems of equations are solved using combinations of Jacobi and advanced multigrid preconditioned conjugate gradient solvers [1,2]. The computational code was SMP parallelized and approximately 14 hours of elapsed time were required for 120 ms of simulation using 50 threads on a p590 IBM Regatta.

This method has been used previously to compute bidomain potentials in cardiac tissue models [3,4,6].

The outputs of the electric potential computations for each point j were the potential values, V_{mj} and ϕ_j, the total current density, $\boldsymbol{J}_j$, the volume associated with the computational point, V_j, and the location of the centroid of the volume in space, $\boldsymbol{x}_j$. The total current density is the sum of the intracellular and extracellular computed values.

2.3 Computing Magnetic Flux Density

It was assumed that the currents were changing sufficiently slowing for the magnetostatic approximation to be valid. The magnetic flux density was then calculated using the Biot-Savart equation:

$$\mathbf{B} = \frac{\mu_0}{4\pi}\int_V \frac{\mathbf{J}\times\mathbf{r}}{|\mathbf{r}|^3}dV$$

Although Gauss' law for magnetism is not explicitly enforced, we assumed that all current paths had been included in the integral/approximation. The distance between a point on the magnetic measurement plane and a point at which a current density is known is $\mathbf{r}$, and the free space permeability is $\mu_0 = 4\pi\times10^{-10}$ H/mm. The components of this integral were approximated as:

$$B_x = \frac{\mu_0}{4\pi}\sum_j \frac{\left(\left(J_y r_z\right)_j - \left(J_z r_y\right)_j\right)}{|\mathbf{r}_j|^3}V_j$$

$$B_y = \frac{\mu_0}{4\pi}\sum_j \frac{\left(\left(J_z r_x\right)_j - \left(J_x r_z\right)_j\right)}{|\mathbf{r}_j|^3}V_j$$

$$B_z = \frac{\mu_0}{4\pi}\sum_j \frac{\left(\left(J_x r_y\right)_j - \left(J_y r_x\right)_j\right)}{|\mathbf{r}_j|^3}V_j$$

These computations were performed using an SMP parallelized calculation code that used the outputs from the potential calculation step described in Section 2.2.

2.4 Model Parameters

Three problems have been solved and are reported here. Problem 1 used a set of effective conductivities that provided an equal anisotropy ratio between the intracellular and the extracellular domains. The nominal anisotropy of problem 2 used effective anisotropies that resulted in different anisotropy ratios between the domains. Problem 3 used the same set of conductivities as the problem 2 but included a fiber direction that rotated through the depth of the tissue.

2.4.1 Effective Conductivities

Effective Conductivity (mS/mm)	Equal Anisotropy Ratio	Nominal Anisotropy
σ_{ix}	0.343	0.2
σ_{iy}	0.0596	0.02
σ_{ex}	0.625	0.8
σ_{ix}	0.109	0.2
bath	2.0	2.0

2.4.2 Fiber Rotation

For the problem with fiber rotation, a fiber angle of 30º (with respect to the x-axis) was defined on the upper tissue surface and a fiber angle of 120º was defined on the lower tissue surface. The angle varied linearly through the depth of the tissue.

2.4.3 Stimulus Currents

A square current pulse of 0.0585 mA was applied for 5 ms. The cathode was located 0.1 mm below the tissue surface. The anode was located in the bath directly below the tissue (Figure 1). To this point in these preliminary results, no effort has been made to systematically determine the threshold current. One reason why the current may be lower than that required for the experimental context is that the volume of the tissue directly depolarized by the cathode in the simulations was 0.0039 mm^3, which may be different to the experimental case.

3.0 Results

Transmembrane potential (V_m) and magnetic flux density fields (B_z, B_x and B_y) are shown over a 30 mm by 30 mm window equivalent to the top surface of the tissue slab. The V_m field is from the top surface of the tissue and has not been depth integrated. The B* fields have been computed on a surface 0.15 mm above the surface of the tissue.

These results do not include any effects from the insulator core on the stimulating electrode.

3.1 Equal Anisotropy Ratio

In this problem, the conductivity values providing an equal anisotropy ratio were used.

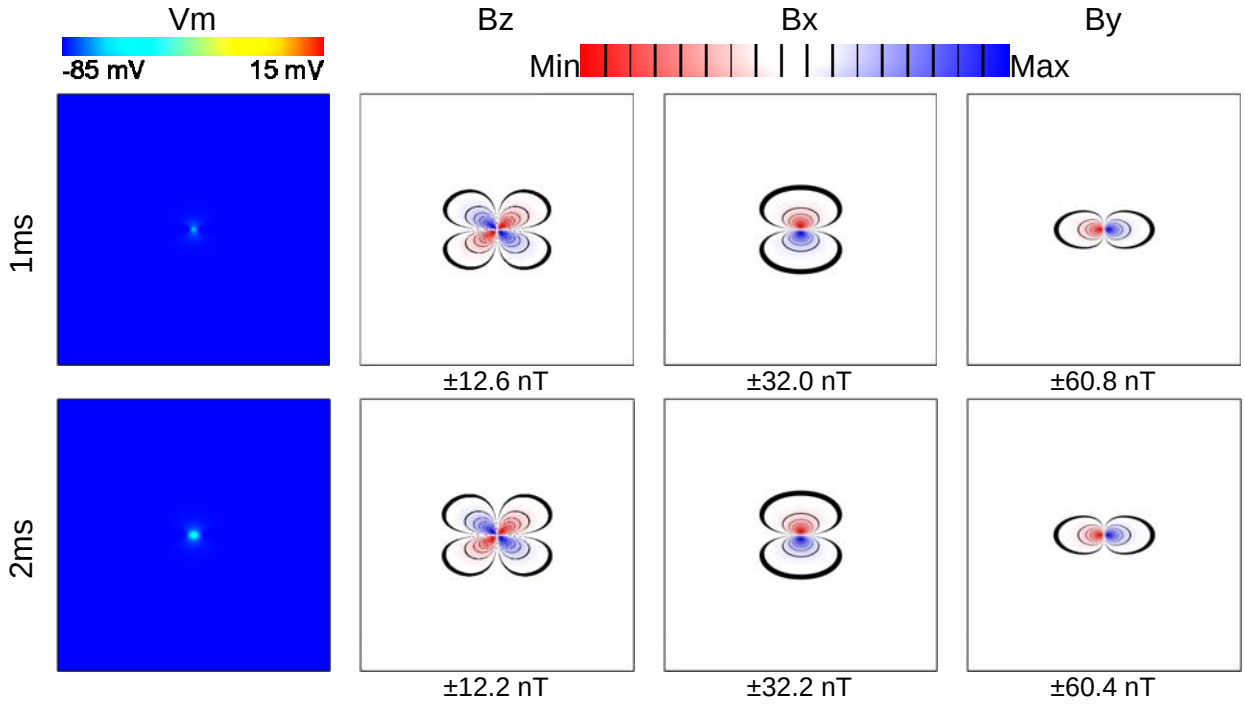

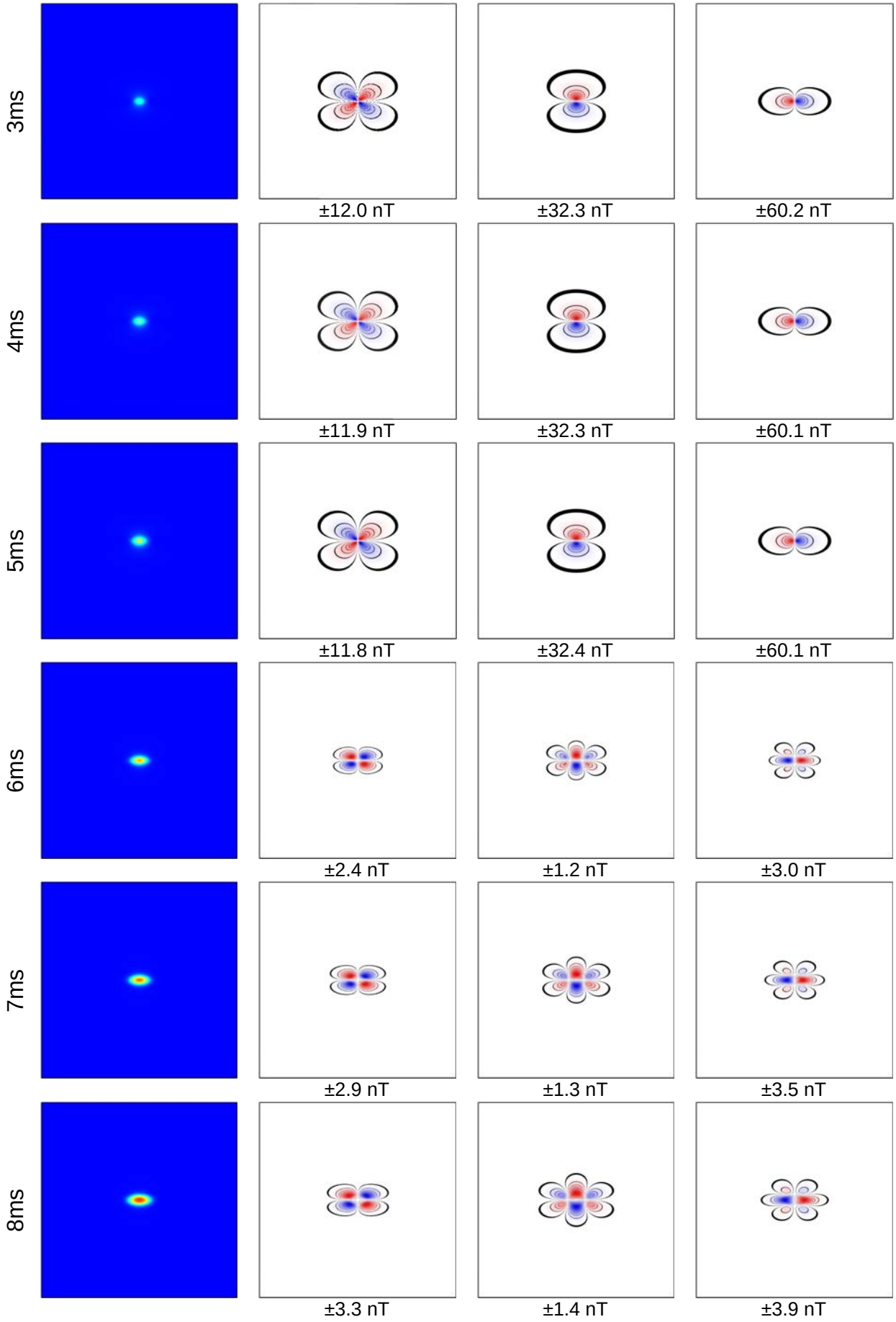
3ms
±12.0 nT
±32.3 nT
±60.2 nT
4ms
±11.9 nT
±32.3 nT
±60.1 nT
5ms
±11.8 nT
±32.4 nT
±60.1 nT
6ms
±2.4 nT
±1.2 nT
±3.0 nT
7ms
±2.9 nT
±1.3 nT
±3.5 nT
8ms
±3.3 nT
±1.4 nT
±3.9 nT

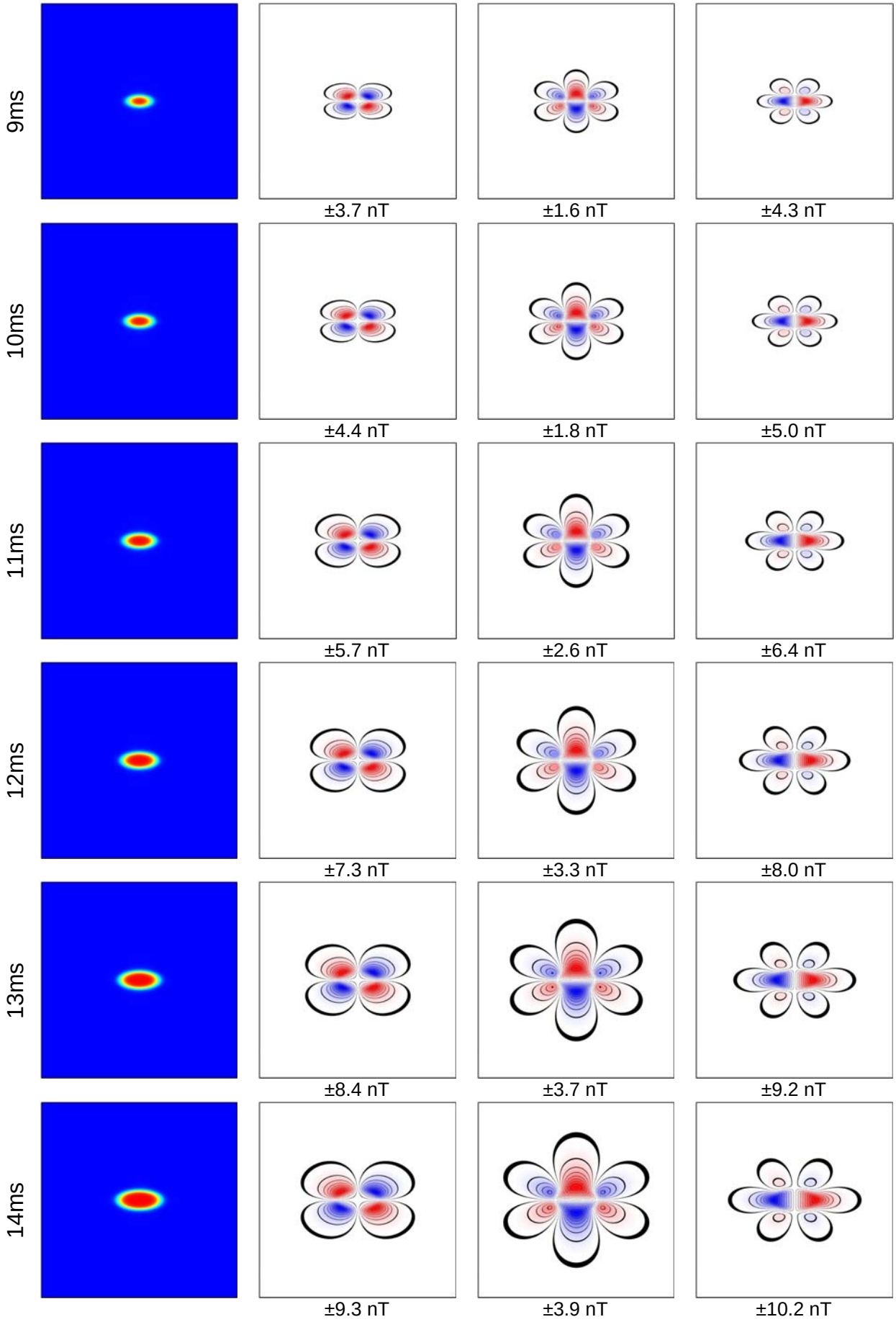
9ms
±3.7 nT
±1.6 nT
±4.3 nT
10ms
±4.4 nT
±1.8 nT
±5.0 nT
11ms
±5.7 nT
±2.6 nT
±6.4 nT
12ms
±7.3 nT
±3.3 nT
±8.0 nT
13ms
±8.4 nT
±3.7 nT
±9.2 nT
14ms
±9.3 nT
±3.9 nT
±10.2 nT

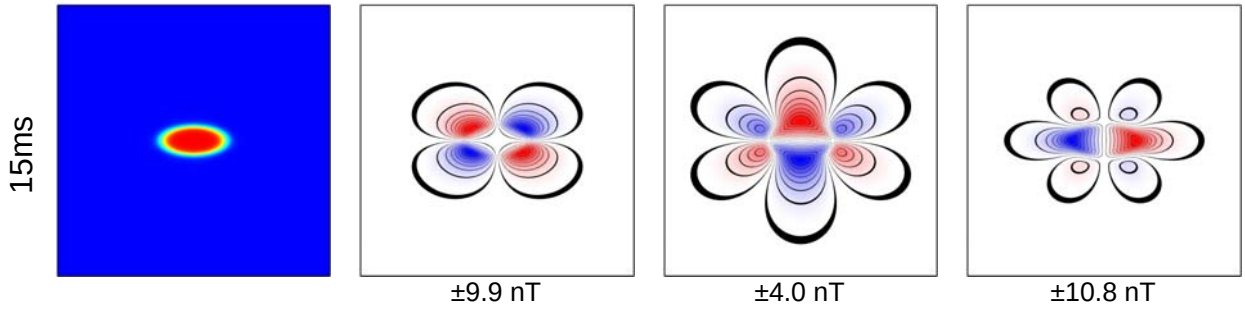

Figure 3. Equal anisotropy ratio: transmembrane potential fields and magnetic flux density fields over 15 ms.

3.2 Nominal Anisotropy Ratio

In this problem, the conductivity values for nominal anisotropy were used. The flux density fields following the termination of the bipolar stimulus have a spatially smaller footprint compared to the equal anisotropy ratio solutions (Section 3.1), corresponding to the smaller extent of activation relative to that problem.

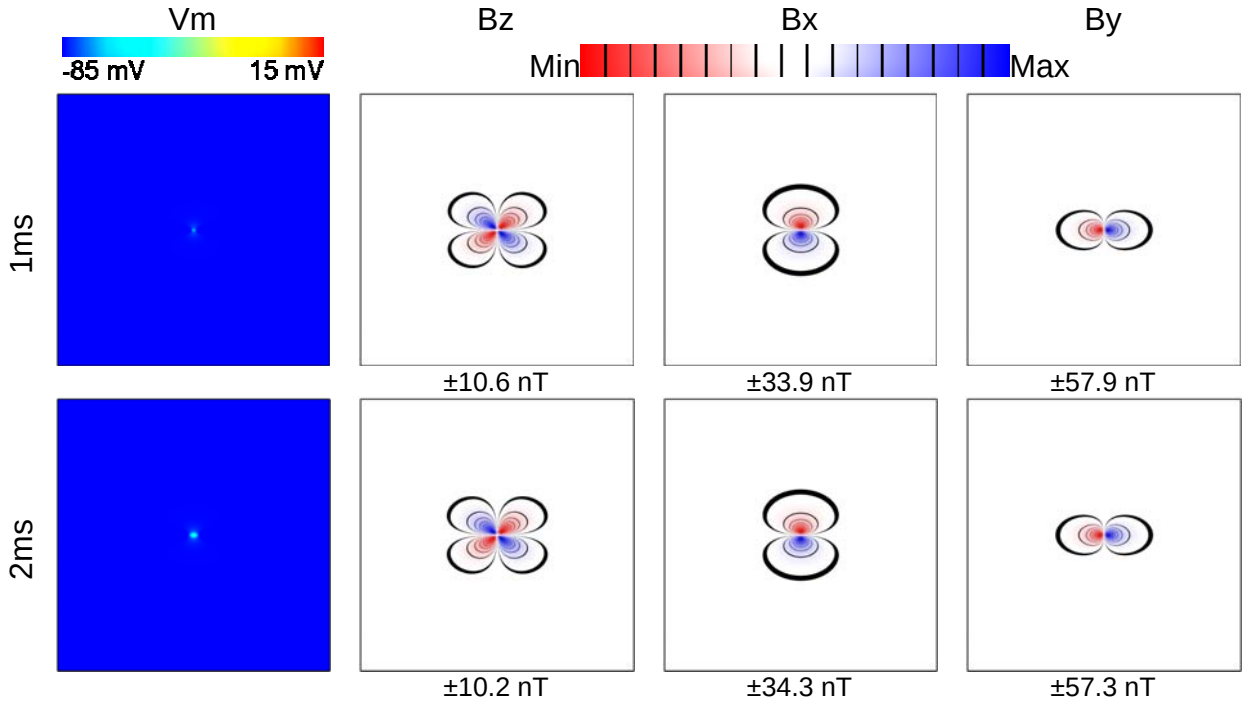

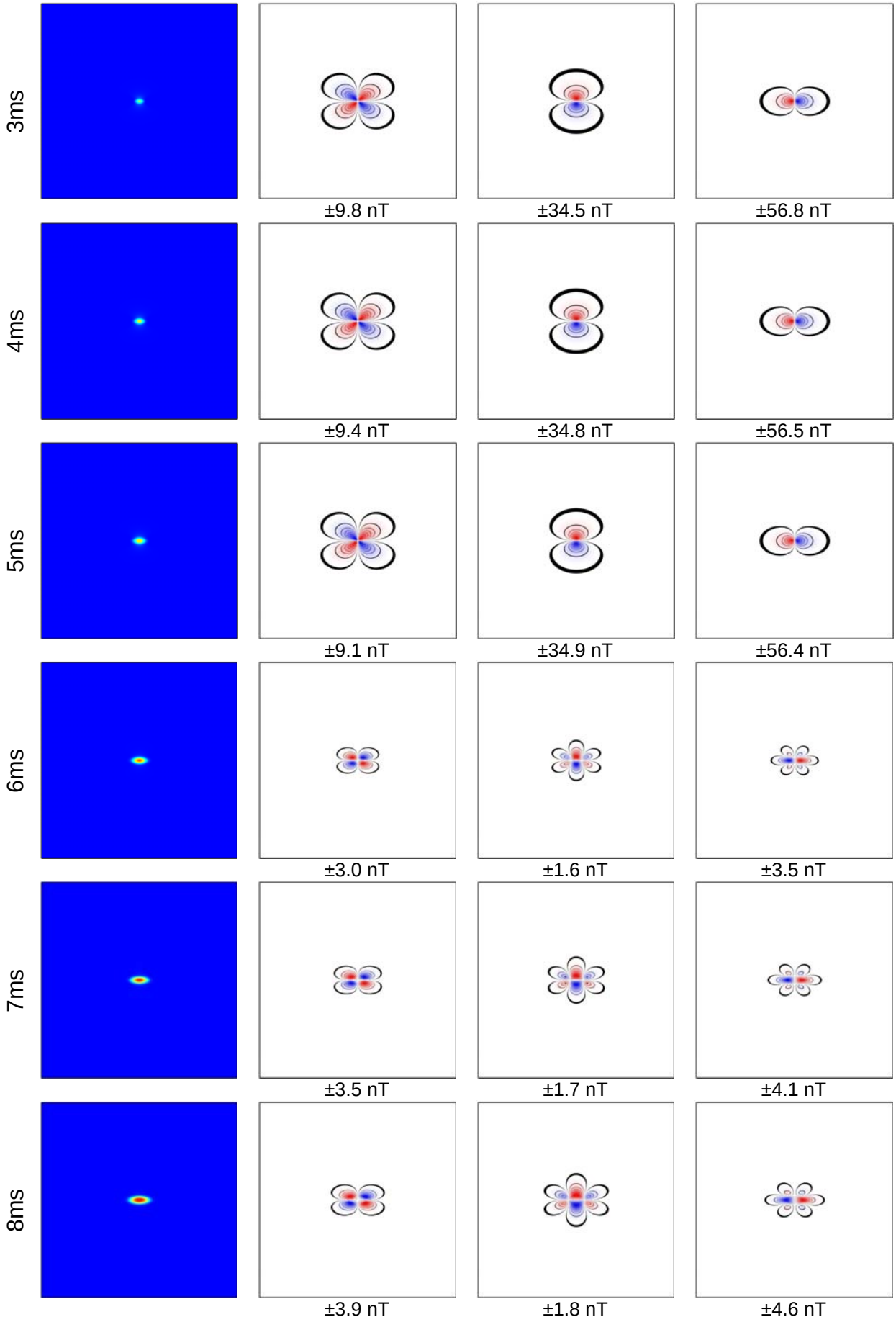
3ms
±9.8 nT
±34.5 nT
±56.8 nT
4ms
±9.4 nT
±34.8 nT
±56.5 nT
5ms
±9.1 nT
±34.9 nT
±56.4 nT
6ms
±3.0 nT
±1.6 nT
±3.5 nT
7ms
±3.5 nT
±1.7 nT
±4.1 nT
8ms
±3.9 nT
±1.8 nT
±4.6 nT

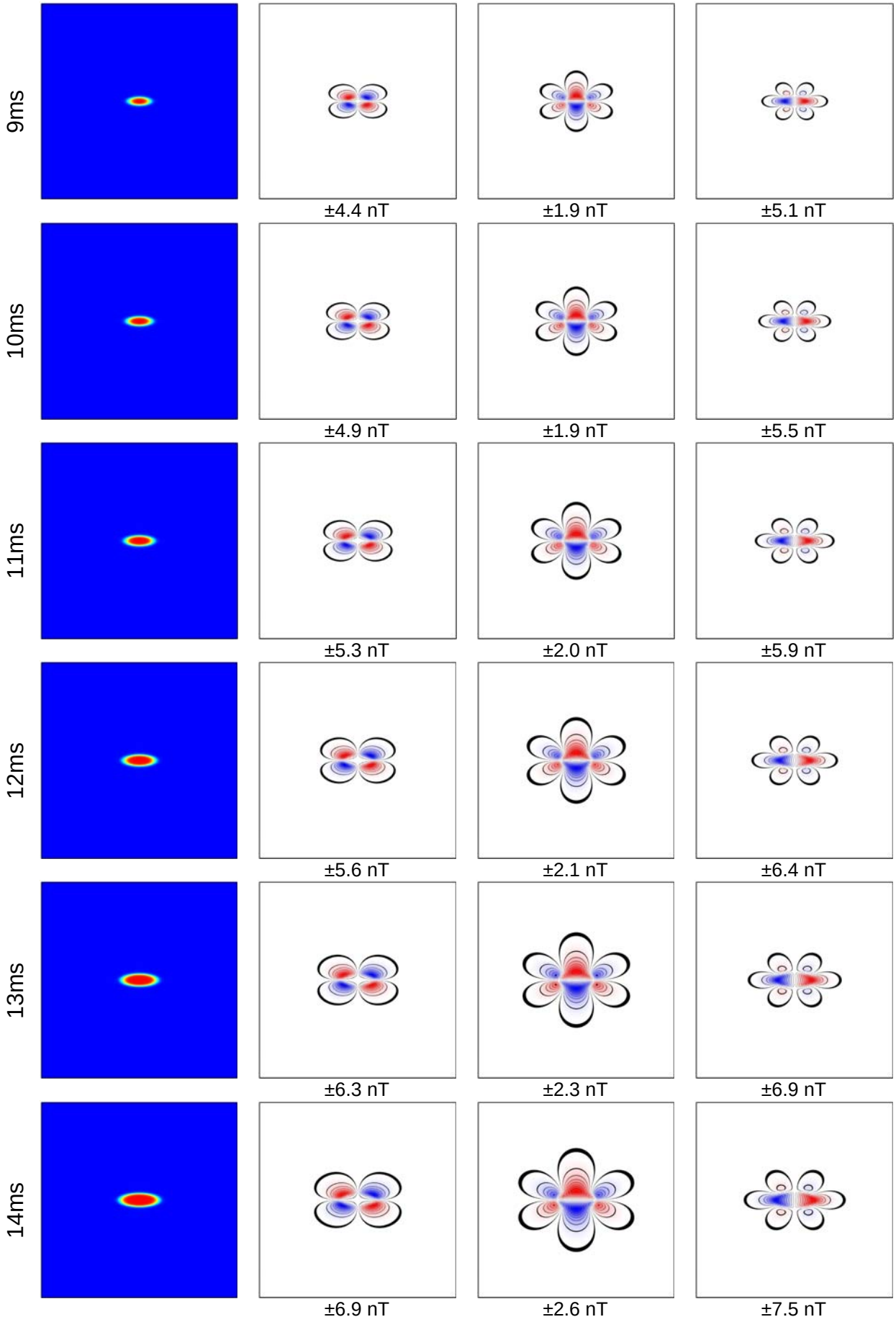
9ms
±4.4 nT
±1.9 nT
±5.1 nT
10ms
±4.9 nT
±1.9 nT
±5.5 nT
11ms
±5.3 nT
±2.0 nT
±5.9 nT
12ms
±5.6 nT
±2.1 nT
±6.4 nT
13ms
±6.3 nT
±2.3 nT
±6.9 nT
14ms
±6.9 nT
±2.6 nT
±7.5 nT

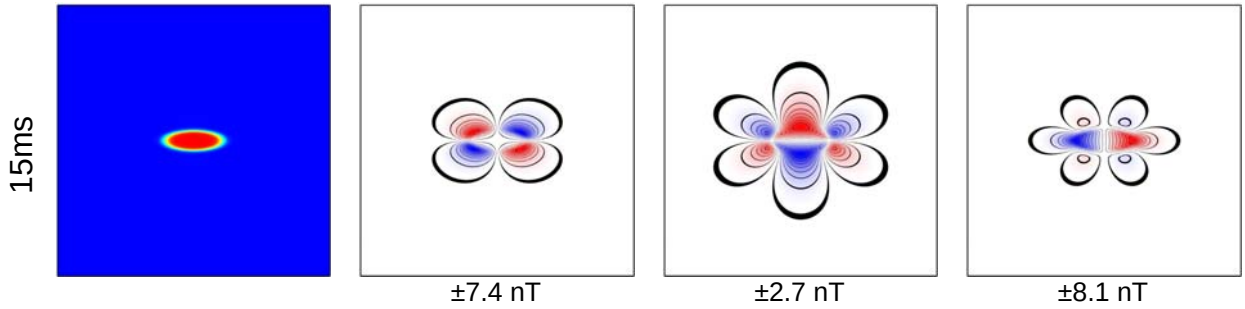

Figure 4. Nominal anisotropy ratio: transmembrane potential fields and magnetic flux density fields over 15 ms.

3.3 Nominal Anisotropy Ratio with Fiber Rotation

In this problem, the conductivity values for nominal anisotropy were used together with a fiber field that rotated from +30º from the x-axis on the top surface of the tissue sample to +120º at the bottom surface. This rotation was more extreme than what would be expected over 1mm of actual tissue thickness, but it served to illustrate that what was observed experimentally likely includes a contribution from tissue rotation.

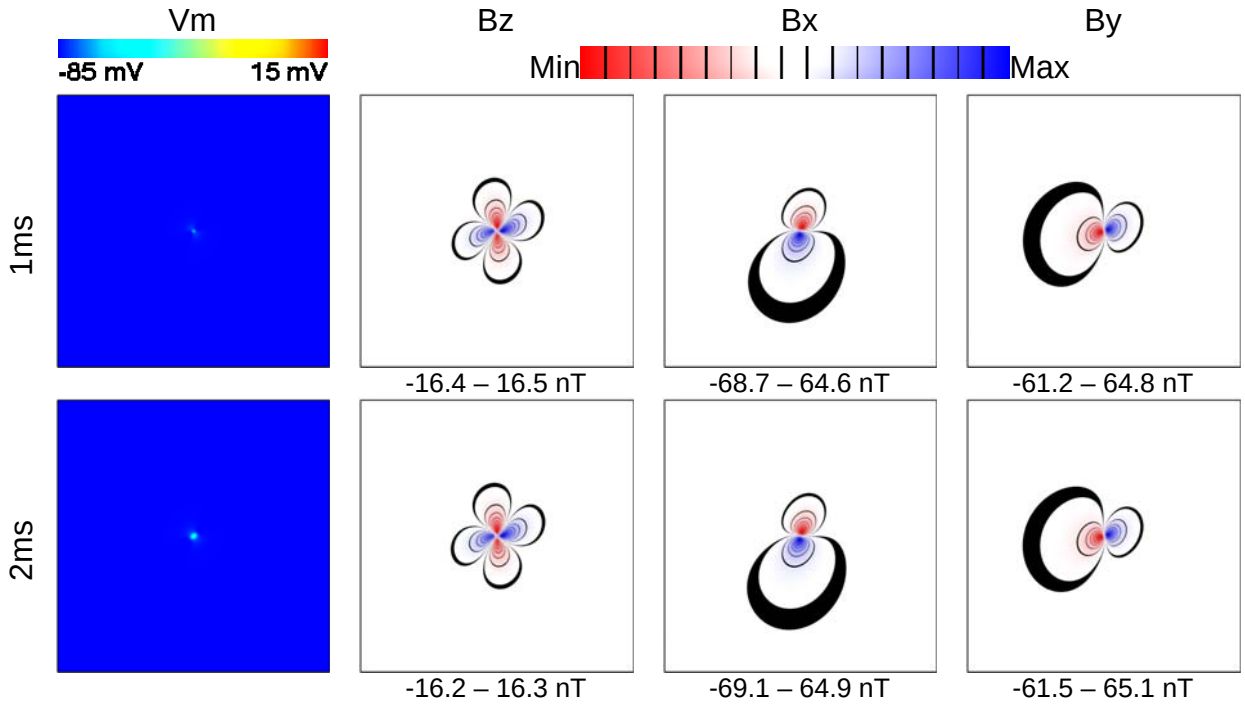

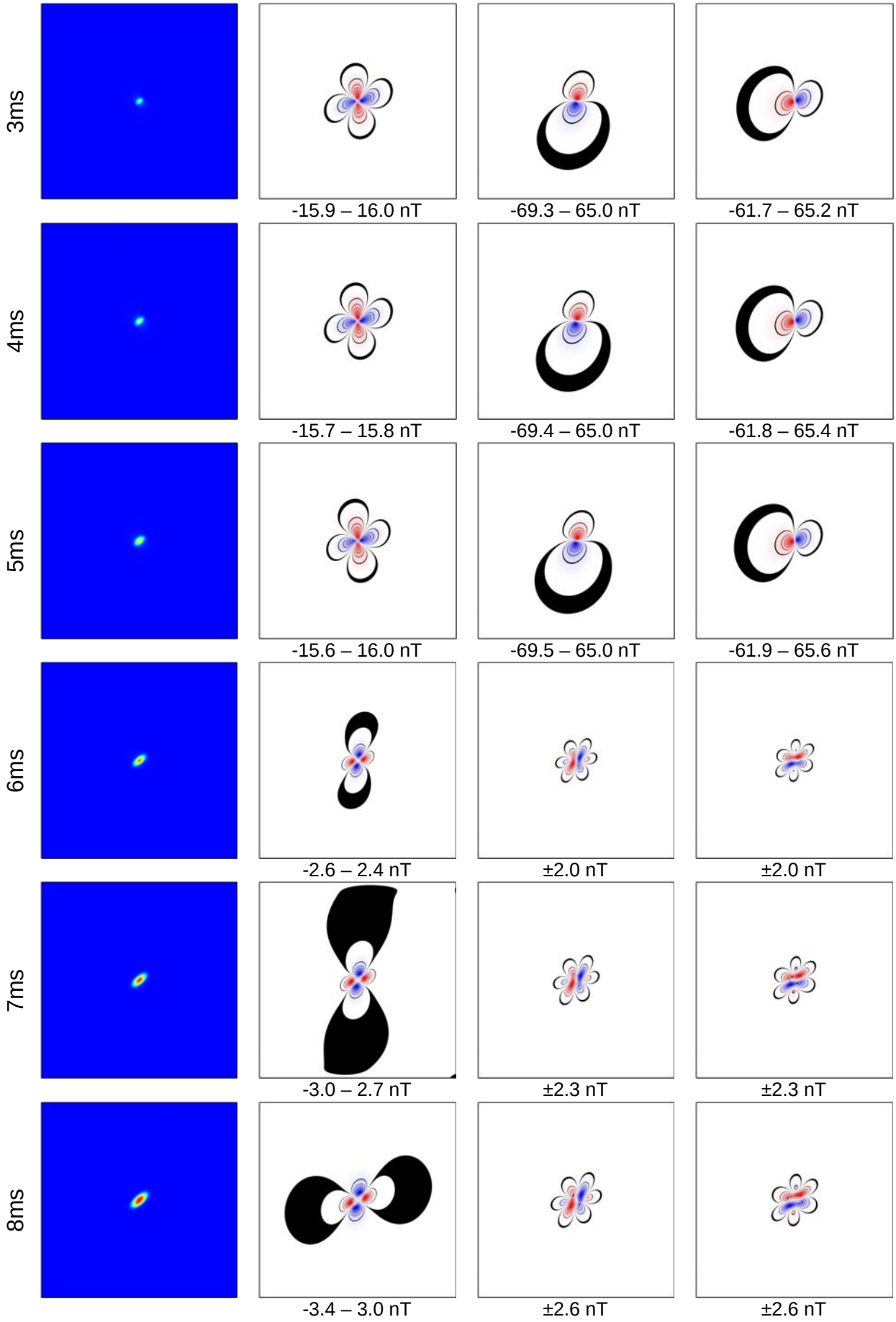
3ms
-15.9 – 16.0 nT
-69.3 – 65.0 nT
-61.7 – 65.2 nT
4ms
-15.7 – 15.8 nT
-69.4 – 65.0 nT
-61.8 – 65.4 nT
5ms
-15.6 – 16.0 nT
-69.5 – 65.0 nT
-61.9 – 65.6 nT
6ms
-2.6 – 2.4 nT
±2.0 nT
±2.0 nT
7ms
-3.0 – 2.7 nT
±2.3 nT
±2.3 nT
8ms
-3.4 – 3.0 nT
±2.6 nT
±2.6 nT

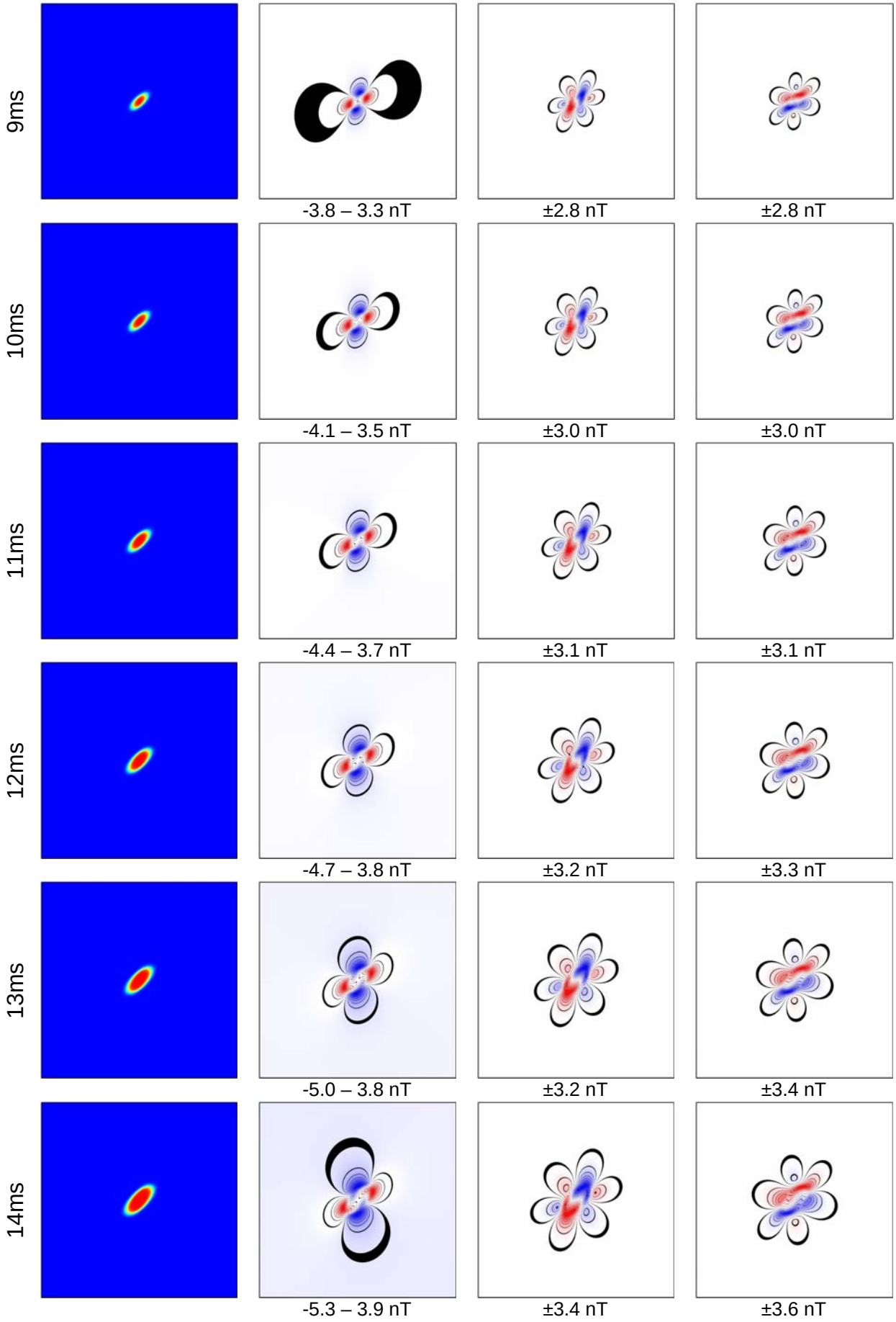
9ms
-3.8 – 3.3 nT
±2.8 nT
±2.8 nT
10ms
-4.1 – 3.5 nT
±3.0 nT
±3.0 nT
11ms
-4.4 – 3.7 nT
±3.1 nT
±3.1 nT
12ms
-4.7 – 3.8 nT
±3.2 nT
±3.3 nT
13ms
-5.0 – 3.8 nT
±3.2 nT
±3.4 nT
14ms
-5.3 – 3.9 nT
±3.4 nT
±3.6 nT

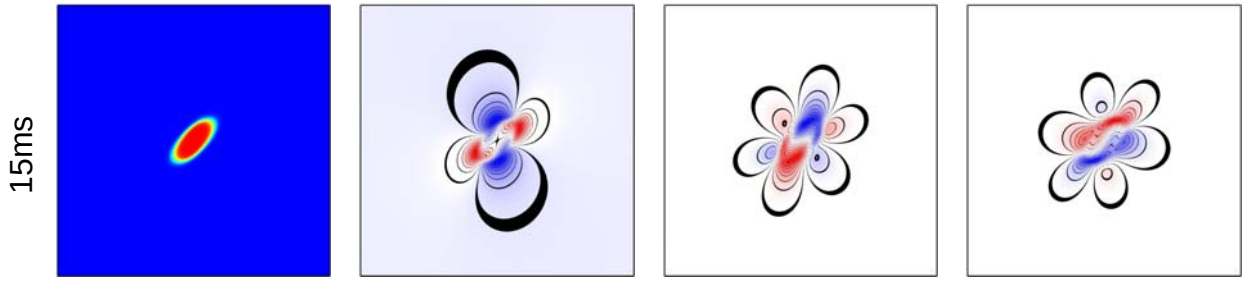

Figure 5. Nominal anisotropy ratio with fiber rotation: transmembrane potential fields and magnetic flux density fields over 15 ms.

4.0 Future Directions

Future work that could be undertaken to improve this model includes:

1. Investigate the effects of using a smaller bath region so that the thickness of the tissue slab can be increased without significantly increasing the number of degrees of freedom in the problem.
2. Include more realistic rotating fibers.
3. Explicitly include the insulator region in the model.

5.0 References

[1] AUSTIN, T., TREW, M., PULLAN, A. 'Solving the Cardiac Bidomain Equations for Discontinuous Conductivities.' *IEEE Transactions on Biomedical Engineering*, 53(7), 1265-1272, 2006.

[2] AUSTIN, T., TREW, M., PULLAN, A. 'A Comparison of Multilevel Solvers for the Cardiac Bidomain Equations,' *Proceedings of the 27th Annual International Conference of the IEEE EMBS, Shanghi, September 1-4*, 2005.

[3] HOOKS, D., TREW, M., SMAILL, B., PULLAN, A. 'Evidence that Intramural Virtual Electrodes Facilitate Successful Defibrillation. Model Based Analysis of Experimental Evidence.' *Journal of Cardiovascular Electrophysiology*, 17(3), 305-311, 2006.

[4] SANDS, G., TREW, M., HOOKS, D., LeGRICE, I., PULLAN, A., SMAILL, B. 'Constructing a Tissue-Specific Model of Ventricular Microstructure' *Proceedings of the 26th Annual International Conference of the IEEE EMBS, San Francisco, September 1-5*, 3589-3592, 2004.

[5] TREW, M., LeGRICE, I., SMAILL, B., PULLAN, A. 'A Finite Volume Method for Modeling Discontinuous Electrical Activation in Cardiac Tissue' *Annals of Biomedical Engineering*, 33(5), 590-602, 2005.

[6] TREW, M., SANDS, G., CALDWELL, B., HOOKS, D., PULLAN, A., SMAILL, B. 'Cardiac Activation and the Impact of a Discontinuous Myocardium. Modeling Studies.' *Proceedings of the 27th Annual International Conference of the IEEE EMBS, Shanghi, September 1-4*, 2005.

[7] TREW, M., SMAILL, B., PULLAN, A. 'What of Cleavage Planes? The State-of-the-Art in Microstructure Modeling of Cardiac Activation.' *International Journal of Bioelectromagnetism*, 7(1), 299-302, 2005.